Pergamon

Int. J. Solids Structures Vol. 35, No. 22, pp. 2861–2875, 1998

0020–7683/98 $19.00 + .00

PII: S0020–7683(97)00178–9

CRACK DETECTION CHARACTERIZATION OF STRAIN SENSING GRIDS

NABIL FARES* and ROULA MALOOF
Polytechnic University, Department of Civil and Environmental Engineering, Brooklyn, NY 11201, U.S.A.

(*Received* 6 *March* 1997; *in revised form* 12 *June* 1997)

Abstract—This paper presents a new probabilistic framework for evaluating measurements to detect anomalies such as cracks. The new framework accounts for the role of errors and the role of policy parameters such as the maximum allowable rate of false alarms and the required minimum probability of detecting critical anomalies. The framework is applied to the detection of cracks using strain sensing grids. This problem is studied and illustrated by examples from the viewpoint of both analysis and design. In analysis, the crack detection capability of a strain sensing grid is probabilistically characterized. In design, the specification of grid spacing and pattern is determined at various operating conditions that include the role of errors, minimum crack size that must be detected and other parameters. The computational techniques used to study strain sensing grids is discussed in detail. The main results indicate that under plausible operating conditions, a relatively large number of strain sensing stations (more than one station per three times the square of the minimum crack size to be detected) is needed when the coefficient of variation of the possible errors exceeds 1%. The implications on the required technology for strain sensing grids to detect cracks is briefly discussed. © 1998 Elsevier Science Ltd. All rights reserved.

1. INTRODUCTION

Recently, there has been an increasing interest in developing smart materials. One characteristic of such materials may be their ability to sense damage (Takagi, 1990). This may be achieved by a variety of sensing techniques (Rogers, 1988; Yin *et al.*, 1996) including static strain measurements (Dunphy *et al.*, 1987). In this study, we will present and apply a rational framework (Fares and Maloof, 1996) for the characterization and design of sensing grids that are used to detect cracks. In our examples, we will assume that we measure strain but we can apply our methodology to different types of measurements.

Surface strain measurements have recently been used as a basis to detect and identify holes (Makabe *et al.*, 1993) or cracks (Chen and Nisitani, 1993) in a plate using a deterministic framework. Another related study was done by Otegui *et al.* (1991) who used strain measurements near a crack to detect the progression of that crack in a weld zone. Other theoretical studies include the use of the Boundary Element Method (BEM) (Bezerra and Saigal, 1993; Ulrich *et al.*, 1966) to identify the location, size and shape of a flaw in a plate or arbitrarily specified geometry based on a relatively large number of measurements on the boundaries of that plate. Finally, Schnur and Zabaras (1992) used a specialized inverse method to determine material properties in a layered elastic medium. All the above studies were deterministic except for Bezerra and Saigal (1993) where they considered the role of random errors in the context of computational experiments in being able to identify the flaw characteristics. However, all the above studies omitted some of the *a priori* important factors that must have an important role in detection or identification. These factors include the following:

(i) *Sensitivity of the measurements to damage*

Cracks are easier to detect if the type, location and number of measurements that we make are highly sensitive to the presence of damage. In particular, the damage must produce sufficiently distinctive measurements that are not present in an undamaged structure. It is

* Author to whom correspondence should be addressed. Tel.: 718 491 9102. Fax: 718 491 9102.

the distinctiveness of measurements that are generated by a damaged structure as compared to an undamaged one that allow us to detect the damage.

We note that for the same type of measurement (e.g. strain), we may vary the location and number of transducers that we use to make such measurements. This is a design specification which we may call the measurement setup. For example, if we use strain gauges distributed in a grid pattern then the design setup may be the size, pattern and spacing of the strain gauges.

(ii) *Modeling and measurements errors*

Errors in either modeling or measurements makes it more difficult to differentiate between data obtained from a damaged structure versus an undamaged one. That is because errors may sufficiently change the expected measurements of the undamaged structure to plausibly look like they came from a damaged one. As the magnitude of errors increase, the intersection between plausible measurements from a damaged and undamaged structure increases. Therefore, errors will affect the reliability of detecting damage in structures.

We can reduce errors by improving our models and by improving the quality and quantity of measurements. For example, by repeating the same measurements, we can reduce sampling errors. Of course, errors cannot be completely eliminated and we must consider the role of errors in determining the limits of our detection capability.

(iii) *The maximum allowable (or chosen) probability of false detection*

To understand why the probability of false detection is a crucial factor, we can consider two limiting cases. If we accept a probability of false detection to be up to (exactly) one then we can raise an alarm at every measurement. This ensures that we will detect or fix any damage that may exist but, of course, is extremely wasteful and the detection decision does not really require any measurements. At the other extreme, if we require the probability of false detection to be zero then we can never raise an alarm. That is because we would always be concerned that even the most damage-distinctive measurements be actually from an undamaged structure due to highly unlikely (but not quite impossible) errors. Such limiting cases may not be realistic but they do show that we must specify the maximum probability of false detection as an important factor in a framework for reliable damage detection.

We will call a specific combination of all the above factors, namely, the type of measurement, measurement setup, potential measurement errors and the chosen probability of false detection to be the detection system. Once the detection system has been chosen and/or determined then we can deduce the detection capability.

In general, a crack detection capability may be characterized by the probabilities of detecting cracks of different sizes and orientations as a function of position. In this study, we will characterize the detection capability as follows: (i) We choose a minimum crack size to be detected, (ii) we choose a minimum probability at which such cracks must be detected and (iii) we determine the regions where cracks at the chosen minimum size will have at least the specified minimum probability of being detected.

In designing strain gauge grids, we are given a user specified maximum rate of false detection, minimum crack size to be detected and minimum probability at which the crack with minimum size must be detected. To design the measurement setup, we must specify the strain gauge size, grid pattern and spacing so that while the maximum rate of false detection is not exceeded, the rate of detecting the minimum crack if it occurs anywhere in the structure at least equals the specified detection probability.

In this paper, we will first describe a new theoretical framework that addresses the factors mentioned above. We will then formulate aspects of this general conceptual framework in mathematical form. Next, we will discuss computational aspects related to applying the mathematical formulation to our particular case of detecting a crack by strain sensing grids. This is then followed by presenting computational results with discussions on the analysis and design of strain sensing grids. Finally, we end this paper with an overall summary of key results and recommendations for future research.

2. FRAMEWORK, MODELS AND TECHNIQUES

In this section, we will describe a new framework that incorporates the factors stated in the introduction to evaluate measurements in order to detect damage. After presenting a general detection framework, we will discuss a specialized mathematical implementation of the framework to a class of models that includes the current problem and, finally, we will describe the models used in this particular study along with some of the corresponding computational techniques.

2.1. *Detection framework*

The process of detecting damage in a structure involves making measurements and then deciding whether these measurements indicate the presence of damage. To do so, the measurements may be combined in an index that we call the anomaly index. This index indicates damage when it exceeds a certain threshold. There are some issues related to converting multiple measurements into an index and to choosing the threshold or critical anomaly index. We will next discuss these issues.

Ideally, an anomaly index should have the properties of a norm whereby the index is zero if and only if the measurements cannot be distinguished from those arising from an undamaged structure. However, there are two factors that complicate such a direct definition of an anomaly index. First, in the absence of error, there may be multiple sets of measurements that can be generated from an undamaged structure. For example, we can get different measurements due to the variation in absolute and relative magnitudes of one or more loads on the same undamaged structure. Second, the presence of error further extends the range of possible measurement that could have been produced by an undamaged structure. In this study, we will address these issues as follows:

(a) Choose a norm or pseudo-norm with the distance between data produced by an undamaged structure and the data available as being a candidate anomaly index.
(b) Minimize the value of all candidate anomaly indices over the "flexible" model parameters that are not directly measured. These parameters could be load magnitudes as well as various internal (hidden) variables related to the model. The obtained "minimum" is defined as the anomaly index.
(c) Assume that model predictions will differ from measurements due to errors. Both measurement and modeling contribute to this error. These errors are then modeled as random variables (RVs). Describing these errors is a separate modeling task whose parameters are estimated based on accumulated experience including *a priori* calibrations.
(d) Calculate the critical anomaly index so that the model of an undamaged structure, in the presence of the assumed errors, has a chosen upper-bound rate of triggering an anomaly. Therefore, the critical anomaly index depends on the model, the magnitude of errors and on the acceptable rate of false detection.

The motivation of the above approach can best be understood in the context of evaluating data based on a model. A modeler naturally tries to get the best fit from his or her model by adjusting unconstrained parameters. However, there is a tradeoff between the complexity of a model (in terms of unconstrained parameters) and the requirement of more accurate measurements. In general, complex models are more useful only when we have highly accurate measurements and when we need highly demanding detection policies. To illustrate this in the context of the above detection framework, we will consider two cases as follows:

(1) The model has a large number of unconstrained parameters. Due to this flexibility we estimate the modeling error to be low because, by adjusting the flexible parameters, it is possible to fit a wide range of data. However, the modeling flexibility also allows the undamaged structural model to fit well data obtained from the damaged structural model at perhaps different values of the "flexible" parameters. In terms of detection, this results in relatively small anomaly indices. If the measurement errors are not

correspondingly low then the critical anomaly index will still be relatively high. Therefore, the anomaly index of most damaged structures will be below critical and very few damaged structures will be detected.

(2) The model is too simple in that it poorly represents the potential measurements. Due to this, we estimate the modeling error to be high. Although, the anomaly index may also be relatively high, the modeling errors lead to a much higher critical anomaly index. Therefore, the anomaly index of most damaged structures will be below critical and very few damaged structures will be detected.

We note that the above framework captures the tradeoff mechanism between modeling complexity and accuracy in measurements. Using the above framework, it may then be possible to establish the level of model complexity (or simplicity) that is appropriate in a particular (detection study) application. In that regard, we are assuming that the appropriate complexity level is the one that maximizes the detection potential in view of the measurement accuracy and the detection policy.

Once the model-measurement-policy system has been identified, it is natural to ask what are the damaged structures that can be detected. Since the model probabilistically characterizes the errors, the answer must also be probabilistically characterized. In particular, we will define the detectable configurations at a specified probability level say β to be those damaged structures whose measurements have a probability of at least β in triggering a detection event. The size of the set of detectable configurations is affected by the choice of measurements, modeling errors, measurement errors and the accepted rate of false detection. Identifying the detectable configurations is very useful in understanding the corresponding tradeoffs and tradeoffs across technologies (e.g. strain vs temperature measurements).

2.2. *Mathematical formulation*

In this section, we formulate a restricted form of the framework discussed above. A more general exposition is given in Fares (1994). First, we will consider models that have only a single adjustable parameter which is the load "p". If we represent the fixed parameters by $\mathbf{g}$, the error by $\mathbf{e}$ and the predicted measurement by $\mathbf{d}$ then these are assumed to be related as follows:

$$\mathbf{d}(p, \mathbf{g}, \mathbf{e}) = p\mathbf{m}(\mathbf{g}) + \mathbf{e} \tag{1}$$

For this class of models, we define the anomaly index "a" as follows:

$$\text{anomaly index} \equiv a(\mathbf{g}, \mathbf{d}) = glb\{\|\hat{\mathbf{d}} - \hat{\mathbf{d}}(p, \mathbf{g})\| : \text{for all } p\} \tag{2}$$

where *glb* denotes the greatest lower bound (minimum in many cases), a carat "$\hat{}$" above a vector indicates it is normalized and the notation $\|\cdot\|$ stands for the root-mean-square norm of the enclosed quantity.

We note that the above choice of anomaly index disregards information related to the magnitude of the load. This would be justified if either the load has simply not been measured or if the uncertainty in the load measurement is much higher than those related to the strain measurements. This last event could occur due to uncertainties in measuring the load or due to modeling uncertainties. The modeling uncertainties can occur when deformation fields are expected to vary at length scales much larger than the spacing of the strain sensing elements but much smaller than the overall structural dimensions. For example, measurements of surface movements near a fault zone may disregard overall plate tectonic load estimates in evaluating the progression of slip on the nearby fault. Another example relates to strain measurements near a weld zone on a cylindrical pressure vessel that may be used to monitor possible cracks. In that cases, the pressure load in the vessel may be accurately known, but local geometrical details, such as pipe inlets and outlets, that are not explicitly modeled may lead to uncertainties in the local effective load magnitude.

In cases where the load is available and is accurately measured and modeled, then we may separately test the consistency of the measured load and that infered from the local strain measurements in an effort to detect anomalies. Alternatively, we may adopt another definition of the anomaly index that includes the role of the load magnitude (Fares, 1994).

In the numerical studies, the error "**e**" is assumed to have the following characterization with statistical parameter "v":

$$e_i \text{ is } N(0, vpm_i) \quad \text{and } e_i\text{'s are independently normally distributed} \tag{3}$$

If we denote by "$1-\alpha$" the maximum rate of false detection then observed data $\mathbf{d}^{\text{observed}}$ would trigger a detection event when the anomaly index exceeds the critical anomaly index k_α given below (Fares, 1994):

$$\text{detection event} \Leftrightarrow glb\{\|\hat{\mathbf{d}}^{\text{observed}} - \hat{\mathbf{d}}(p, \mathbf{g}_b, v)\| : \text{for all } p\} \leqslant k_\alpha \tag{4a}$$

where:

$$k_\alpha(\mathbf{g}) = lub\{k : Pr[glb\{\|\hat{\mathbf{d}}^{\text{syn}}(\mathbf{p}^{(1)}, \mathbf{g}) - \hat{\mathbf{d}}^{\text{pred}}(\mathbf{p}^{(2)}, \mathbf{g})\| : \text{for all } p^{(2)}\} \leqslant k] \geqslant \alpha \text{ for all } p^{(1)}\} \tag{4b}$$

Due to the difficulty in determining k_α exactly, we will use an upper bound of k_α given by Fares (1994). This upper bound is given as:

$$k_\alpha(\mathbf{g}) \leqslant \frac{v \max_i [m_i(\mathbf{g})]}{\|\mathbf{m}(\mathbf{g})\|} \chi_{\alpha, n_d} \tag{5}$$

where: χ_{α, n_d} is the value at which a Random Variable (RV) that is Chi-distributed with n_d degrees of freedom has a cumulative distribution equal to α.

In the computational studies, the right hand side of the inequality (5) will be used to estimate the critical anomaly index $k_\alpha(\mathbf{g})$. This leads to conservative designs of detection grids because a higher critical anomaly index leads to a lower rate of false alarms.

The mathematical definition of the detectable configurations is complicated. The complexity arises from the definition of the anomaly index and the possibility that, due to errors, the load that generates the data may be different than the one that gives the best fit. If we choose the minimum probability that a detectable configuration must trigger a detection event to be β and the fixed parameters of the undamaged structure to be $\mathbf{g}_b$, then the set of detectable configurations G_β is given by:

$$G_\beta(\mathbf{g}_b, \alpha) = \{\mathbf{g} : Pr[glb\{\|\hat{\mathbf{d}}(p^{(1)}, \mathbf{g}, \mathbf{e}) - \hat{\mathbf{d}}(p^{(2)}, \mathbf{g}_b, 0)\| : \text{for all } p^{(2)}\} \geqslant k_\alpha(\mathbf{g}_b)] \geqslant \beta \text{ for all } \mathrm{p}^{(1)}\} \tag{6}$$

The exact identification of the detectable configurations is a difficult computational problem even in this specialized class of models. In order to decrease the computational requirements, we will instead obtain subsets of the detectable configurations. A damaged configuration in a subset of the detectable configuration will also have a probability of at least β in being detected. If we use a uniform approach in identifying such subsets then such an approach would also be useful in characterizing the detection capability across different applications. Of course, such an approach would not be the most complete characterization but is a step in the right direction. One class of subsets of the detectable configurations may be identified through compliance with the following relatively simple inequality (Fares, 1994):

$$(\|\hat{\mathbf{m}}(\mathbf{g})-\hat{\mathbf{m}}(\mathbf{g}_b)\| \geqslant k_\alpha(\mathbf{g}_b)+k_\beta(\mathbf{g})) \Rightarrow \begin{pmatrix}\text{Probability that data generated by}\\ \text{configuration } \mathbf{g} \text{ will be detected}\end{pmatrix} \geqslant \beta \quad (7)$$

In the computational studies, we will use the condition (7) to approximately identify the detectable configurations. This leads to conservative designs of detection grids since the detection capability of a given grid will then be underestimated.

2.3. *Design of detection grids*

The problem of designing strain sensing grids to detect cracks may be described by specifying the design assumptions, constraints and parameters. The main design assumptions in this study are:

(a) A single straight sharp crack may exist in a plate. The size of the plate is assumed to be much larger than the size of the crack (see Fig. 1).
(b) The plate is in tension with the load axis perpendicular to the crack.
(c) The plate behaves linearly elastically.
(d) The modeling and measurement errors are well represented by random variables that are characterized by the statement labeled as relation (3).

We note that deviations from the above assumptions may be partially absorbed by increasing the estimate of the modeling errors. Another approach is to use more complex models to describe the problem but that is outside the scope of the current study. Figure 2 illustrates the general geometry and setup that applies to the problem.

The design constraints are mainly related to the detection policy. In this study, the main design constraints are as follows:

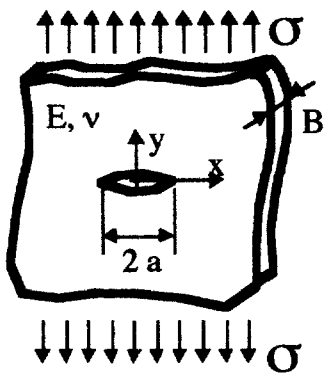

Fig. 1. Straight through-crack in a plate subject to tension. The material is linear elastic characterized by Young's modulus E and Poisson's ratio ν.

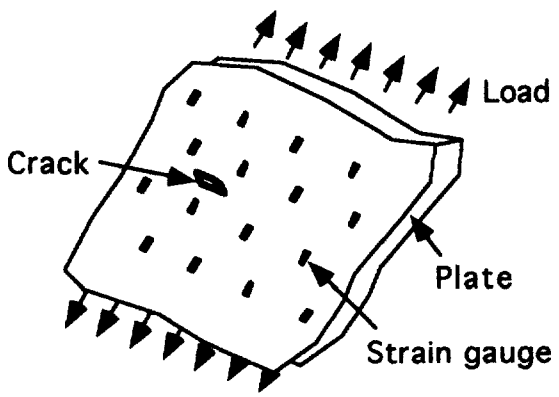

Fig. 2. Array of strain gauges used to detect a possible crack in a plate subject to tension.

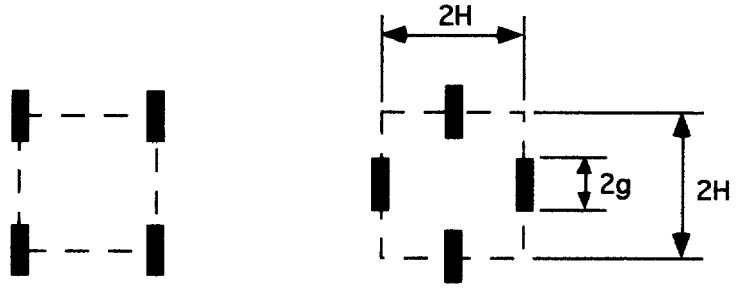

Fig. 3. Two basic patterns are considered for the strain gauge grids. The corner grid pattern shown in (a) and the cross grid pattern shown in (b). The geometry of this pattern is parameterized by the gauge size "$2g$" and the gauge spacing "$2H$".

(a) The rate of false detection must not exceed a specified value denote by $1-\alpha$.
(b) Cracks whose size are greater than a specified minimum denoted by "$2a$" must be detected anywhere in the plate with a probability at least equal to a specified value denoted by β.

In order to meet the design constraints, we will assume that strain tensors (e.g. strain gauges) are distributed in a regular pattern as a grid over the plate. Therefore, the design parameters are:

(a) The pattern of the strain sensors: in this study, we will consider two patterns (see Fig. 3): (i) a square pattern with strain sensors at the corner of each square and (ii) a square pattern with strain sensors at the midpoints of each side. We will refer to these patterns as corner and cross grids, respectively.
(b) The spacing of the strain sensors: in this study, this will be expressed as multiplies of the smallest crack size that must be detected at high probability. This reference length scale is appropriate because cracks significantly perturb static strain patterns only relatively close to them. Therefore, we expect the spacing of strain sensing elements to have length scales comparable to the minimum crack sizes that must be detected.
(c) The gauge size of the strain sensors: in terms of strain gauges, this is the size of the strain gauge and corresponds to the length over which strains are averaged. For convenience, we will normalize the gauge size by the gauge spacing.

The purpose of a design is to obtain design specifications that satisfy all the design constraints. In this case, the design specifications are the pattern, the spacing and the size of the strain sensors. Of course, optimal designs are those that maximize specified objectives, which in this problem may be the number of gauges per unit area required to achieve the detection capability. In this study, we will not obtain mathematically optimal designs but simply estimate the best designs that can be calculated in view of the various approximations and assumptions. However, we emphasize that while the calculated design specifications are not optimal, they have partially been optimized and do satisfy all the design constraints.

2.4. *Computational techniques*

The model that predicts the strain measurements due to a crack in a plate is available analytically (e.g. Hellan, 1984). Detailed assumptions of this analytic result have been outlined in the previous section. The elastic displacement fields in a plate shown in Fig. 1 may be expressed in terms of a Mushkelishvilli's potential for plane stress as follows:

$$\phi(z,a) = \sqrt{z^2 - a^2} \tag{8a}$$

$$2\mu u_x = \frac{\sigma}{2}\frac{1-\nu}{1+\nu} Re(\phi) - \frac{\sigma}{2} y\, Im(\phi') - \frac{\sigma}{2} x \tag{8b}$$

$$2\mu u_y = \sigma \frac{1}{1+v} Im(\phi) - \frac{\sigma}{2} y\, Re(\phi') + \frac{\sigma}{2} y \tag{8c}$$

where $z = x + Iy$ (I is $\sqrt{-1}$), "$2a$" is the crack size, "μ" is the shear modulus, "v" is Poisson's ratio, u_x and u_y are the displacements in the x and y directions, respectively, σ is the magnitude of the remotely applied uniaxial stress, *Re* and *Im* indicate the real and imaginary parts. The displacements due to a crack at a translated position may be obtained from eqns (8) by a simple shift in the coordinates. The field variable that is needed in this study is the displacement in the y-direction from which we can get the average axial strain "$\varepsilon_{\text{average}}$" in a strain gauge aligned with the axis of the load as follows:

$$\varepsilon_{\text{average}} = \frac{u_y \text{ at top edge} - u_y \text{ at bottom edge}}{\text{length of strain gauge}} \tag{9}$$

The displacement field u_y is shown plotted in Fig. 4 in a 3-D plot as a function of x and y. In the absence of a crack, the displacement field will have the shape of an inclined plane. Figure 4 indicates that the crack perturbs this "inclined-plane" displacement pattern only in a relatively small neighborhood. This localization is quantified in Fig. 5 which shows the percent difference in axial strain (ε_{yy}) between a cracked solid and a similarly loaded intact plate. The result shown in Fig. 5 suggests that when the combined modeling and measurement errors may be of the order of 10% then a crack is unlikely to be detected by a strain gauge grid whose spacing exceeds a few times the crack size. We note that in Fig. 5, the total area where the absolute difference in strains exceeds 10% is about 2.74 times the square of the crack length (i.e. $2.74 \times (2a)^2$). This suggests that if the various sources of error add up to about 10% then the order of magnitude of the spacing should not exceed $\sqrt{2.74} \approx 1.7$ times the crack size. This estimate does not account for specified limits on the rate of false alarm nor does it account for the need to avoid "blind spots". A more precise quantification of the required spacing per minimum crack size that takes both these factors into account in a systematic framework was discussed in the previous section and will be further discussed below.

In the process of designing the strain gauge grid, we must be able to analyze the crack detection capability of a particular grid. The design process will then repeatedly use this analysis capability to identify specifications. Specifically, if we are given a particular crack size, an estimate of the errors, the required upper-bound on the rate of false alarms and the minimum probability at which the crack size must be detected, then we must be able to

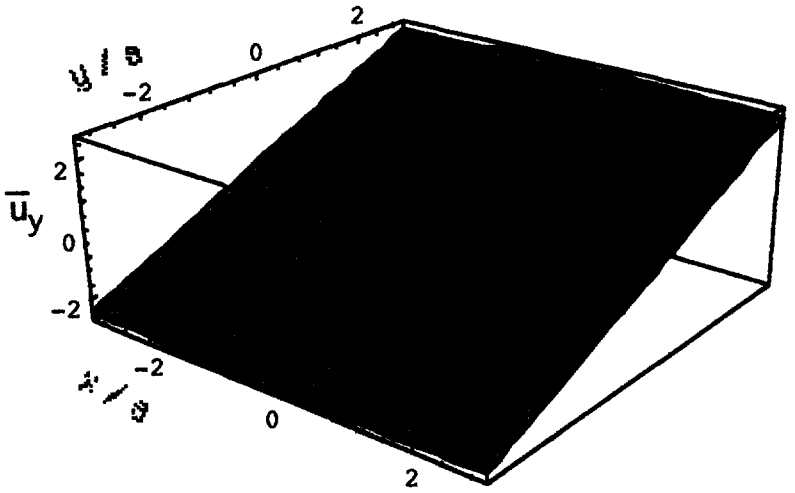

Fig. 4. The axial displacement in a plate with a crack subject to tension shows only a local perturbation surrounding the crack as compared to a plate without a crack. The axis of the tensile load is along the y-axis and the crack lies along the x-axis between $x/a = -1$ and $x/a = 1$.

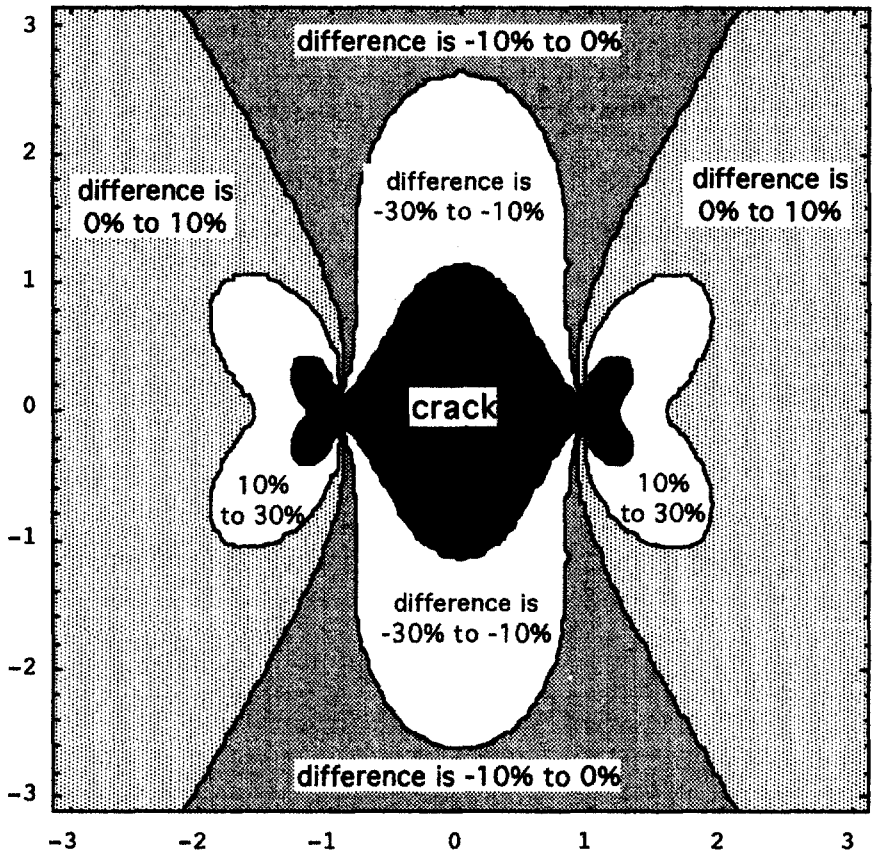

Fig. 5. A comparison of the axial strain in a plate with a crack as compared to one without a crack both subject to tension. Regions where the percentage change is 10% or more is in a relatively small neighborhood of the crack.

determine locations of such a crack on the plate that satisfy those conditions. We will call such locations the detectable region. We characterize the detectable regions by finding its boundaries. An estimate of these boundaries are locations where relation (7) is an equality. This computational task involves having $\mathbf{g}_b$ parameterizing an uncracked plate and searching for the set of parameters $\mathbf{g}$ that makes relation (7) an equality. Details of this computational task are discussed below.

To identify the boundaries of the detectable region, we start by searching along an arbitrarily chosen line in the neighborhood of the crack until we bracket a zero (i.e. relation (7) is negative on one side and positive on the other). We then use bisection to identify a first point on the boundary of the detectable region. The rest of the points are obtained by searching for an adjacent point on the boundary in a particular direction. To do that, we choose a point in the negative region of relation (7) (point A in Fig. 6), another in the positive region of relation (7) (point B in Fig. 6) and a third point that forms an equilateral triangle with the other two in a specific traversal direction (point C in Fig. 6). The third point (i.e. point C) will be either in the negative region, positive region or on the boundary. If point C is not on the boundary then a new point on the boundary may be found by bisection using either A and C or B and C depending on the sign of C. Initially, points A and B shown in Fig. 6 may be obtained along the line which was used to bracket the first boundary point. Subsequently, points A and B of Fig. 6 may be obtained along the normal to the line joining the current and previous boundary points (i.e. points "n-1" and "n" in Fig. 6).

Occasionally, the technique discussed above will fail either because the sides of the triangle A–B–C in Fig. 6 are too large (Fig. 7(a)) or because of a cusp point on the boundary of the detectable region (Fig. 7(b)). In either case, the sign of the points A, B and C will be

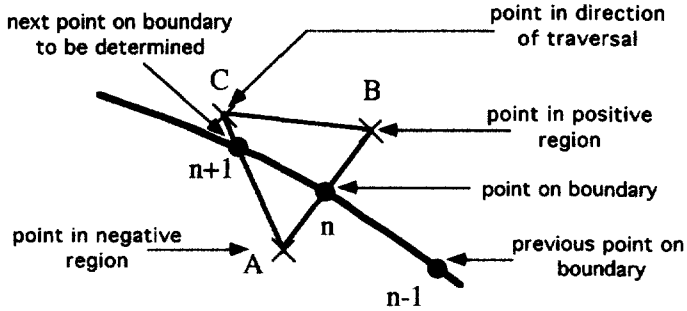

Fig. 6. The computational technique of searching for points on the boundary of the detectable region starts by calculating values of the discriminating function at points A, B and C that lie in the neighborhood of a known boundary point "n". The next point on the boundary "$n+1$" is then determined by bisection along either line A–C as in this case or in some other cases along line B–C.

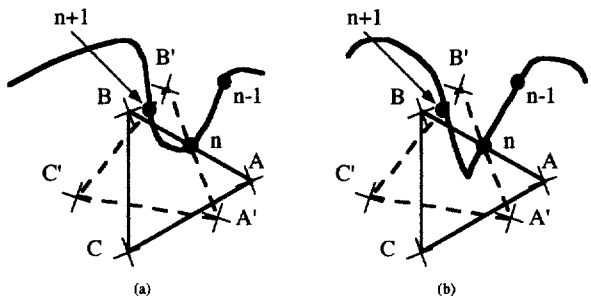

Fig. 7. In some cases, the computational technique of searching for points on the boundary of the detectable region is unable to proceed to the bisection phase of the algorithm because all three points A, B and C have the same sign as illustrated in (a) and (b). This may be fixed by gradually rotating the initial search points A, B and C until new points A′, B′ and C′ are found that allow bisection to work.

the same and therefore bisection cannot be used to find the next point. This problem may be solved by choosing a sufficiently small size for the distance between A and B (identified by trial and error) and by choosing new points A′, B′ and C′ that are obtained by gradually rotating the triangle A–B–C (as shown in Fig. 7(a) and 7(b)). Eventually, with a sufficiently small initial triangle A–B–C, a rotated triangle A′–B′–C′ may be found that allows a new boundary point to be determined by bisection.

In some cases, the region of interest may be multiply connected. The multiple boundaries may be determined one at a time by combining the above technique with a global grid search. Of course, we must carefully choose (i.e. by trial and error and eventually experience) the various parameters involved in the algorithms based on the above descriptions of this computational technique. These parameters include the size of the "search triangle" (i.e. A–B–C in Figs 6 and 7), the increment at which triangle A–B–C rotates if necessary, the conditions at which a search ends (e.g. contour closure, too many steps, etc.) and various parameters associated with the bisection and grid search methods.

Once the boundary or boundaries of a region are determined then the area of that region can also be determined using a simple line integral based on the divergence theorem, specifically:

$$\text{Area} = \oint_C x n_x \, ds = \oint_C y n_y \, ds \tag{10}$$

where n_x and n_y are the direction cosines of the normal to the contour C enclosing the region of interest, "s" is an arc length variable and C is the contour (or contours properly traversed) along the boundary.

In this study, we will sometimes remove part of the detectable region that lies outside a quadrant identified by the center of a sub-array of four strain gauges that make up the grid and then we determine the coverage area. This allows us to determine the percent of a quadrant that is detectable. If a quadrant is fully (i.e. 100% of the area) detectable then, by symmetry and periodicity, the whole region covered by the strain gauge grid is detectable. By varying the size of the crack, we can determine the minimum crack size in which the detectable region covers all the quadrant. Therefore, we can tabulate minimum crack sizes for given operating conditions of grid spacing, gauge size, error levels, maximum rate of false alarm and minimum detection probability. Such tables then form the basis for designing strain gauge grids to be used for detecting cracks.

3. DISCUSSION OF RESULTS

In all the computational studies presented in this paper, we choose $\alpha = 0.95$ and $\beta = 0.95$. This means that we are choosing the maximum rate of false alarms to be 5% and the probability of detecting cracks of the specified minimum size that occur in the detectable regions to be at least 95%. The effect of varying α and β have been presented by Fares and Maloof (1996) in a related study but is outside the scope of the present results.

Figures 8 and 9 show the detectable regions as shaded areas for the corner and cross grid patterns, respectively. Each of Figs 8 and 9 show cases for four different crack sizes labeled (a), (b), (c) and (d) corresponding to relative crack sizes to gauge spacing of 0.15, 0.25, 0.35 and 0.45, respectively. The coefficient of variation characterizing the error when obtaining the results of Figs 8 and 9 is 0.01 (i.e. $v = 0.01$). Figures 8 and 9 both indicate

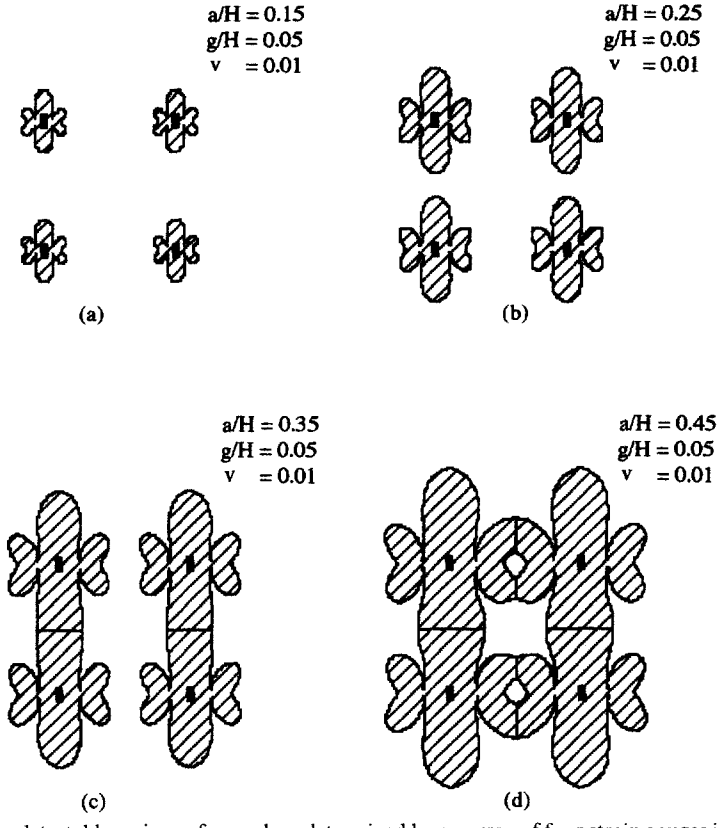

Fig. 8. The detectable regions of a crack as determined by an array of four strain gauges in a corner grid pattern are shown in figures (a), (b), (c) and (d) at relative crack sizes $a/H = 0.15$, 0.25, 0.35 and 0.45, respectively. The maximum rate of false alarms is chosen to be 5%, the minimum probability of detection is chosen to be 0.95, the gauge size to spacing is fixed at 0.05 and the coefficient of variation of the errors is 0.01.

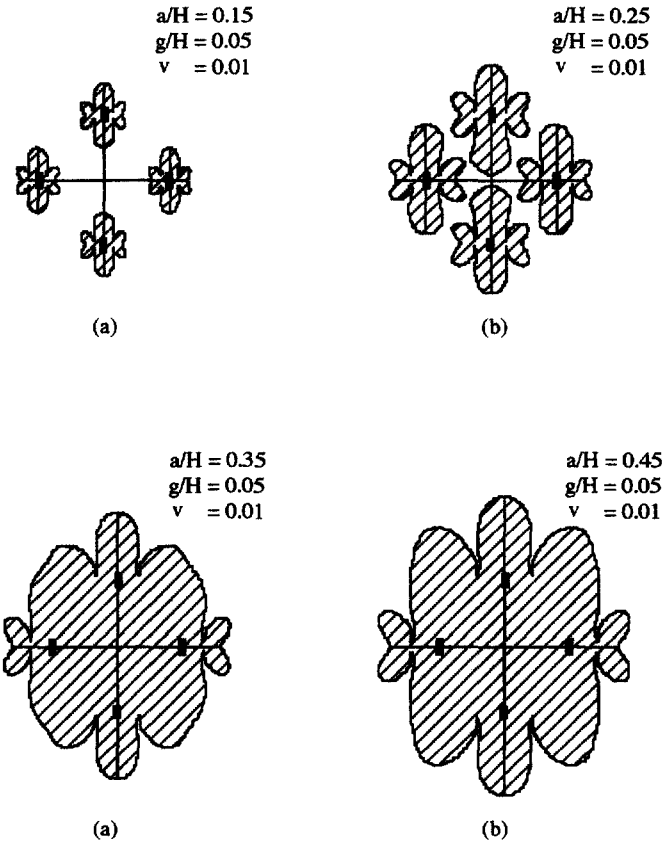

Fig. 9. The detectable regions of a crack as determined by an array of four strain gauges in a cross grid pattern are shown in figures (a), (b), (c) and (d) at relative crack sizes $a/H = 0.15$, 0.25, 0.35 and 0.45, respectively. The maximum rate of false alarms is chosen to be 5%, the minimum probability of detection is chosen to be 0.95, the gauge size to spacing is fixed at 0.05 and the coefficient of variation of the errors is 0.01.

that when the crack size is small enough then each gauge detects cracks only in its neighborhood. This occurs when a crack significantly perturbs the strain at only one strain gauge. By significant we mean that the perturbation can be discerned above the level of random errors. In that case, we get identical disconnected shapes for the detection region with area that is expected to increase as the square of the crack size. This is seen in Figs 10 and 11 at sufficiently small crack sizes. We note that this trend is somewhat disrupted when the crack size is about the same size as or smaller than the strain gauge length. This disruption occurs because of the interaction of three length scales, namely, the strain gauge size, the crack size and the gauge spacing. When the crack size becomes sufficiently bigger than the gauge size then the detection region becomes insensitive to the gauge size (Fig. 11).

If the crack size is sufficiently large then the detectable regions surrounding the individual strain gauges will overlap and interact. This occurs when a crack can significantly and simultaneously perturb the strain at two or more strain gauges. Once there is overlap between the detectable regions surrounding individual strain gauges then the increase in the detectable area is expected to change differently than when there is no overlap (Figs 10 and 11). Figure 10 and 11 show that after an interval of being proportional to $(2a)^2$, the area of the detection region grows faster than $(2a)^2$, reaches a maximum and then the rate of increase with $(2a)^2$ gradually decreases. The maximum in these figures occurs before full coverage of a quadrant.

In terms of detection capabilities, Fig. 8 suggests that the detectable region may never reach full coverage of a quadrant. In fact, full coverage for the corner grid pattern is not possible for the following reason. If the center of a crack occurs right at the center of the four strain gauges (shown in Fig. 3(a)) then the strain at all the four gauges will be uniformly

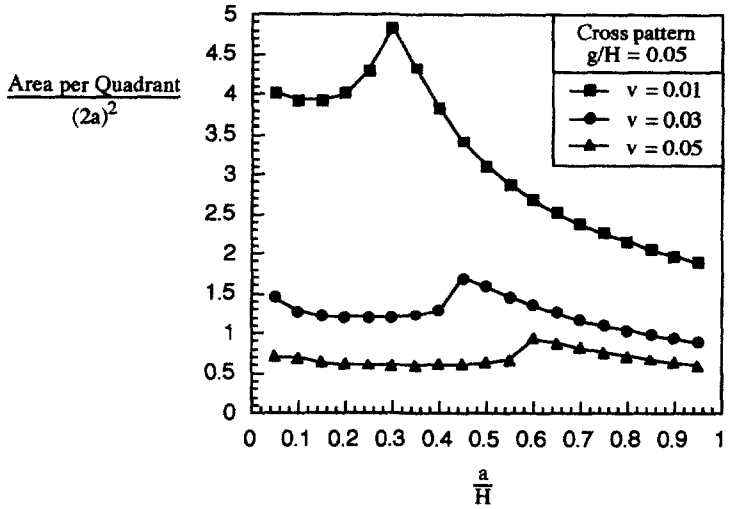

Fig. 10. The ratio of (high probability) detectable areas (per quadrant) over the square of the crack size is plotted vs the ratio of crack size to gauge spacing at three values of the coefficient of variation ($v = 0.01$, $v = 0.03$ and $v = 0.05$).

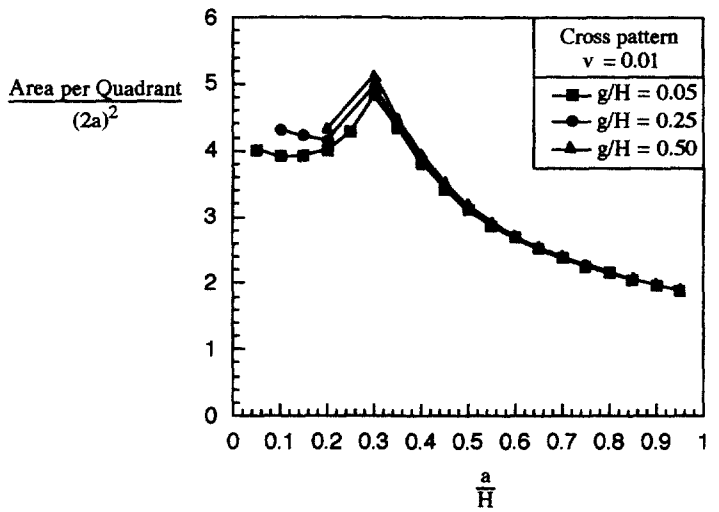

Fig. 11. The ratio of (high probability) detectable areas (per quadrant) over the square of the crack size is plotted vs the ratio of crack size to gauge spacing at three values of the relative gauge size ($g/H = 0.05$, $g/H = 0.25$ and $g/H = 0.50$). The plot indicates that the gauge size plays a minor role as long as it is smaller than the crack size.

amplified. This uniform amplification cannot be distinguished from uniform strain amplification due to an increase in the load magnitude. Since the anomaly index disregards amplitude information in the measurements then a crack at the center of the strain gauges will never be detected. For this reason, the corner grid configuration will not be further considered in this study. By contrast, Fig. 9 shows that, with the cross grid pattern, the detectable region does achieve full coverage of a quadrant. In such a configuration, a crack in the center amplifies the strain at the two gauges at its sides (i.e. left and right gauges) while reducing the strain at the other two. Therefore, the cross grid pattern may detect a crack at the center of the four gauges and does so as shown in Fig. 9.

In order to design a strain sensing grid at fixed $\alpha = \beta = 0.95$, we must specify the grid spacing that achieves full detection coverage as a function of the minimum detectable (at high probability) crack size ($2a$) and the level of errors characterized by the coefficient of variation "v". The grid spacing will scale proportionately to the minimum crack size when this minimum is much larger than the gauge size or when we fix the ratio of gauge size to

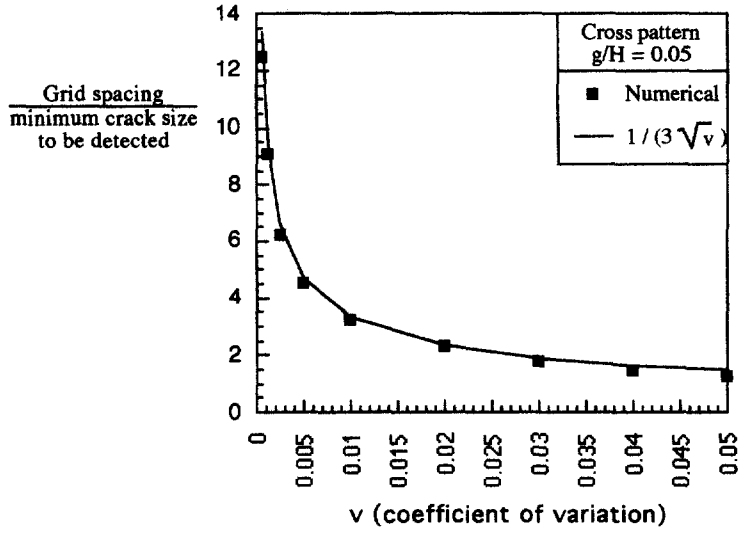

Fig. 12. In order to design a strain sensing grid, the required spacing between the strain gauges over the minimum crack size to be detected must be determined when given the level of errors (both theoretical and experimental). This combined error is characterized by the coefficient of variation "v". The detection process is subject to the following requirements. The rate of false alarms must not exceed 5% ($1-\alpha$ in the text) and the probability of detecting the minimum sized crack must be at least 95% (β in the text).

gauge spacing. Of course, the spacing must decrease if the level of errors increases. Therefore, a design formula, table or plot must relate the ratio of grid spacing over minimum crack size to be detected with the level of expected errors characterized by the coefficient of variation "v". Figure 12 presents such a design plot showing both computational results and a simple curve-fitted formula. Given an estimate of the coefficient of variation "v", Fig. 12 gives the required grid spacing as a multiple of the minimum crack size to be detected. We note that these results were obtained for $\alpha = \beta = 0.95$ with a cross-grid square pattern. Experience with a related study shows that the results are only weakly sensitive to α and β when they range between 0.90 and 0.99.

Figure 12 indicates that when the coefficient of variation is greater than about 1% then the required grid spacing for reliable detection requires a relatively large number of sensors per given area. Such a dense strain sensing grid may be possible with fiber optic embedded meshes or with non-contact full-field measurements such as speckle laser-interferometry (in structural applications) and satellite based radar interferometry (in geophysical applications) but is unlikely to be practical with strain gauges. Alternatively, if very low errors (i.e. the coefficient of variation is less than 1%) can be achieved then crack detection grids using strain gauges may be practical. Such low errors may, in some cases, be achieved by *a priori in situ* calibrations which decrease theoretical errors and by averaging a large number of measurement samples which decreases the measurement errors.

4. CONCLUSIONS

This paper presented the motivation, principles and mathematical formulation of a new framework for detecting anomalies such as cracks. The primary motivation includes explicitly accounting for the role of theoretical and experimental errors in detection and allowing explicit control of policy-related parameters. Policy-related parameters include the maximum allowable rate of false alarms and the probability of detecting the class of anomalies of interest. This framework was then applied to the detection of cracks using strain sensing grids. This problem was studied and illustrated by examples from the viewpoint of both analysis and design. In analysis, we identify the region where a given crack size has a specified minimum probability of being detected. In design, we determine the

strain sensor spacing required for having all the region being able to detect a (minimum) specified crack size at a specified minimum probability of detection.

There is a lot of further research that is needed to explore the proposed new framework and to fully characterize the detection capability of strain sensing grids. In the case of strain sensing grids, we may explore the role of policy parameters, the possibility of multiple simultaneous load application, the role of crack eccentricity relative to the load axis as well as many other factors. In the case of the new framework, the list of further research is very extensive. This includes developing further techniques to identify the detectable configurations, exploring alternative definitions of the anomaly index, handling larger sets of measurements (e.g. time varying signals) and developing a comprehensive theory dealing with model calibrations.

Acknowledgements—The authors would like to thank Professor M. Iskander and Professor C. Santamarina for useful discussions and acknowledge NSF support under award number 9209391.

REFERENCES

Bezerra, L. M. and Saigal, S. (1993) A boundary element formulation for the inverse elastostatics problem (IESP) of flaw detection. *International Journal of Numerical Methods in Engineering* **36,** 2189–2202.

Chen, D.-H. and Nisitani, H. (1993) Detection of a crack by body force method. *Engineering Fracture Mechanics* **45**(5), 671–685.

Dunphy, J. R., Meltz, G. and Elkow, R. M. (1987) Distributed strain sensing with a twin core fibre optic sensor. *ISA Transactions* **26**(4), 7–10.

Fares, N. and Maloof, R. (1966) A probabilistic framework for detecting and identifying anomalies. *Probabilistic Engineering Mechanics*, submitted.

Fares, N. (1994) A new framework to detect anomalies and to identify configurations—application to part-through cracks. NSF progress report.

Hellan, K. (1984) *Introduction to Fracture Mechanics*. McGraw-Hill, Appendix B, p. 231.

Makabe, C., Kaneshiro, H. and Itokazu, M. (1993) An inspection of fatigue crack extension based on strain information. *Engineering Fracture Mechanics* **45**(5), 655–662.

Papoulis, A. (1991) *Probability, Random Variables, and Stochastic Processes*. McGraw-Hill.

Rogers, A. J. (1988) Distributed optical fibre sensors for the measurement of pressure, strain and temperature. *Phys. Rep.* **169**(2), 99–143.

Scales, J. A. and Gersztenkorn, A. (1988) Robust methods in inverse theory. *Inverse Problems* **4,** 1071–1091.

Schnur, D. S. and Zabaras, N. (1992) An inverse method for determining elastic material properties and a material interface. *International Journal of Numerical Methods in Engineering* **33,** 2039–2057.

Takagi, T. (1990) A concept of intelligent materials. *J. Intell. Mater. Syst. Struct.* **1,** 149–156.

Ulrich, T. W., Moslehy, F. A. and Kassab, A. J. (1966) Boundary element method-based pattern search solution for a class of inverse elastic problems. *International Journal of Solids and Structure* **33**(15), 2123.

Yin, L., Wang, X.-M. and Shen, Y.-P. (1996) Damage-monitoring in composite laminates by piezolelectric films. *Computers and Structures* **59**(4), 623.